



Vestibular CCK signaling drives motion sickness–like behavior in mice

Pablo Machuca-Márquez^{a,1}, Laura Sánchez-Benito^{a,b,1}, Fabien Menardy^a, Andrea Urpi^a, Mònica Girona^a, Emma Puighermanal^a, Isabella Appiah^a, Richard D. Palmiter^{c,d,2,3} , Elisenda Sanz^{a,b,2,3}, and Albert Quintana^{a,b,e,2,3} 

Contributed by Richard Palmiter; received March 28, 2023; accepted August 23, 2023; reviewed by Simon M. Luckman and Linda Rinaman

Travel can induce motion sickness (MS) in susceptible individuals. MS is an evolutionary conserved mechanism caused by mismatches between motion-related sensory information and past visual and motion memory, triggering a malaise accompanied by hypolocomotion, hypothermia, hypophagia, and nausea. Vestibular nuclei (VN) are critical for the processing of movement input from the inner ear. Motion-induced activation of VN neurons recapitulates MS-related signs. However, the genetic identity of VN neurons mediating MS-related autonomic and aversive responses remains unknown. Here, we identify a central role of cholecystokinin (CCK)-expressing VN neurons in motion-induced malaise. Moreover, we show that CCK VN inputs onto the parabrachial nucleus activate *Calca*-expressing neurons and are sufficient to establish avoidance to novel food, which is prevented by CCK-A receptor antagonism. These observations provide greater insight into the neurobiological regulation of MS by identifying the neural substrates of MS and providing potential targets for treatment.

motion sickness | vestibular | CCK neurons | malaise | optogenetics

Motion sickness (MS) is an unpleasant autonomic physiological condition that occurs in healthy individuals undergoing passive or even illusory motion. MS signs and symptoms include pallor, cold sweating, yawning, retching and vomiting, vertigo, anorexia, drowsiness, and even severe pain (1–5). MS is highly conserved among species (4, 6–9). Thus, while still debated (10), it has been posited that MS may be the by-product of an evolutionary mechanism acting as an early toxin-ingestion warning system leading to reduced metabolism (hypothermia and drowsiness), expulsion of the toxin (vomiting), and future avoidance of the ingested substance (6).

It is widely accepted that MS arises from conflicts between actual visual/vestibular sensory inputs and the expected motion and body position information based on past memories (11–13). Accordingly, the necessity of a functional vestibular system for the development of MS was identified long ago (14, 15). Movement-related information processed by the vestibular organ in the inner ear is relayed directly to the medullo-pontine vestibular nuclei (VN). Compelling evidence demonstrates that VN neurons are central to MS neurobiological regulation by showing that activation of VN neurons through provocative motion reproduced MS-like autonomic alterations in rats and mice (16–18). In addition, diseases that affect VN function are associated to autonomic dysregulation such as vertigo, nausea, and vomiting (19).

The role of the VN in the control of the body orientation system, mainly by means of vestibular reflexes at the ocular, head, neck, and spinal levels, has been well described (20). Furthermore, vestibular outputs have been shown to modulate blood pressure with posture change (21, 22). However, how vestibular function governs motion-induced changes in other MS-mediated responses, such as hypolocomotion, appetite suppression, loss of body temperature, or acquisition of a conditioned taste avoidance (CTA), is still unknown (3, 4, 8, 16, 17, 23–25). Mapping of neuronal activity after provocative motion has identified potential neural substrates for vestibular-induced physiological responses, such as the nucleus of the solitary tract (NTS), paraventricular nucleus of the hypothalamus, parabrachial nucleus (PBN), central amygdala, dorsal raphe nucleus, locus coeruleus, and area postrema (16, 17). Among them, both the NTS and PBN are known to process visceral sensory input in the brainstem (26) and receive direct connections from the VN (27–29).

Excitatory neurons are the main projection-neuron type in the VN (30) and have been suggested to participate in autonomic responses after hypergravity (31) and postural imbalance (32). Furthermore, provocative-motion stimuli activate glutamatergic vesicular glutamate transporter 2 (VGLUT2)-expressing VN neurons that in turn project axons to nuclei such as the PBN (33–35). Thus, we hypothesized that genetically defined,

Significance

We live in an age where travel is paramount. However, one of the most disabling conditions inherent to traveling is motion sickness (MS). While studies have underscored the role of the vestibular system in the development of MS, the neuronal populations involved in motion-induced malaise remain largely unknown. Here, we describe the vestibular pathways eliciting MS responses and identify a key role for cholecystokinin (CCK)-expressing vestibular neurons. We reveal that a vestibulo-parabrachial (VN-PBN) CCKergic projection is sufficient to induce conditioned taste avoidance, likely through the activation of calcitonin gene-related peptide-expressing PBN neurons. Finally, we underscore the role of CCK-A receptor signaling as a druggable target to treat MS, providing insight on the neurobiological substrates of MS.

Author contributions: P.M.-M., L.S.-B., F.M., A.U., M.G., E.P., and I.A., performed research and analyzed data; R.D.P. supported initiation of this project, designed research, and wrote the paper; and E.S. and A.Q. performed research, analyzed data, provided funding, and wrote the paper.

Reviewers: S.M.L., The University of Manchester; and L.R., Florida State University.

Competing interest statement: A patent for the use of CCK-A receptor antagonists as a treatment for MS has been filed.

Copyright © 2023 the Author(s). Published by PNAS. This open access article is distributed under [Creative Commons Attribution-NonCommercial-NoDerivatives License 4.0 \(CC BY-NC-ND\)](https://creativecommons.org/licenses/by-nc-nd/4.0/).

¹P.M.-M. and L.S.-B. contributed equally to this work.

²E.S. and A.Q. contributed equally to this work.

³To whom correspondence may be addressed. Email: palmiter@uw.edu, elisenda.sanz@uab.cat, or albert.quintana@uab.cat.

This article contains supporting information online at <https://www.pnas.org/lookup/suppl/doi:10.1073/pnas.2304933120/-DCSupplemental>.

Published October 17, 2023.

glutamatergic neuronal (sub)populations and circuits in the VN would be sufficient and/or necessary to develop MS-induced autonomic regulation and/or aversive learning. To that end, we used cell-type-specific transcriptomics combined with optogenetic and chemogenetic approaches to identify the underlying vestibular circuitry of MS-induced responses.

Results

Glutamatergic Vestibular Neurons Sustain Motion-Induced Autonomic Responses. Assessment of MS in mice is hindered by the lack of emetic reflex and difficulty to unequivocally identify nausea (5, 8, 36). However, behavioral and autonomic signs of

MS are consistently observed in mice subjected to rotatory or gravitational paradigms (8, 16–18). Thus, we sought to establish a rotational paradigm sufficient to develop robust MS-like symptoms (Fig. 1A). Four repeated 1-min, 4-g accelerations (spin stimulation) consistently induced transient hypolocomotion (Fig. 1B and *SI Appendix, Fig. S1A*). Furthermore, a significant decrease in food intake was observed in food-deprived mice after spin stimulation compared to controls (Fig. 1C), in line with the appetite suppression observed in MS (3, 4, 8, 16, 18, 24). In addition, a decrease in core body temperature, another classical MS response (3, 4, 8, 17, 24, 25), was observed after the rotational stimulus compared to controls, with a maximum temperature difference of 4 °C that occurred ~17.5 min after rotation onset (Fig. 1D).

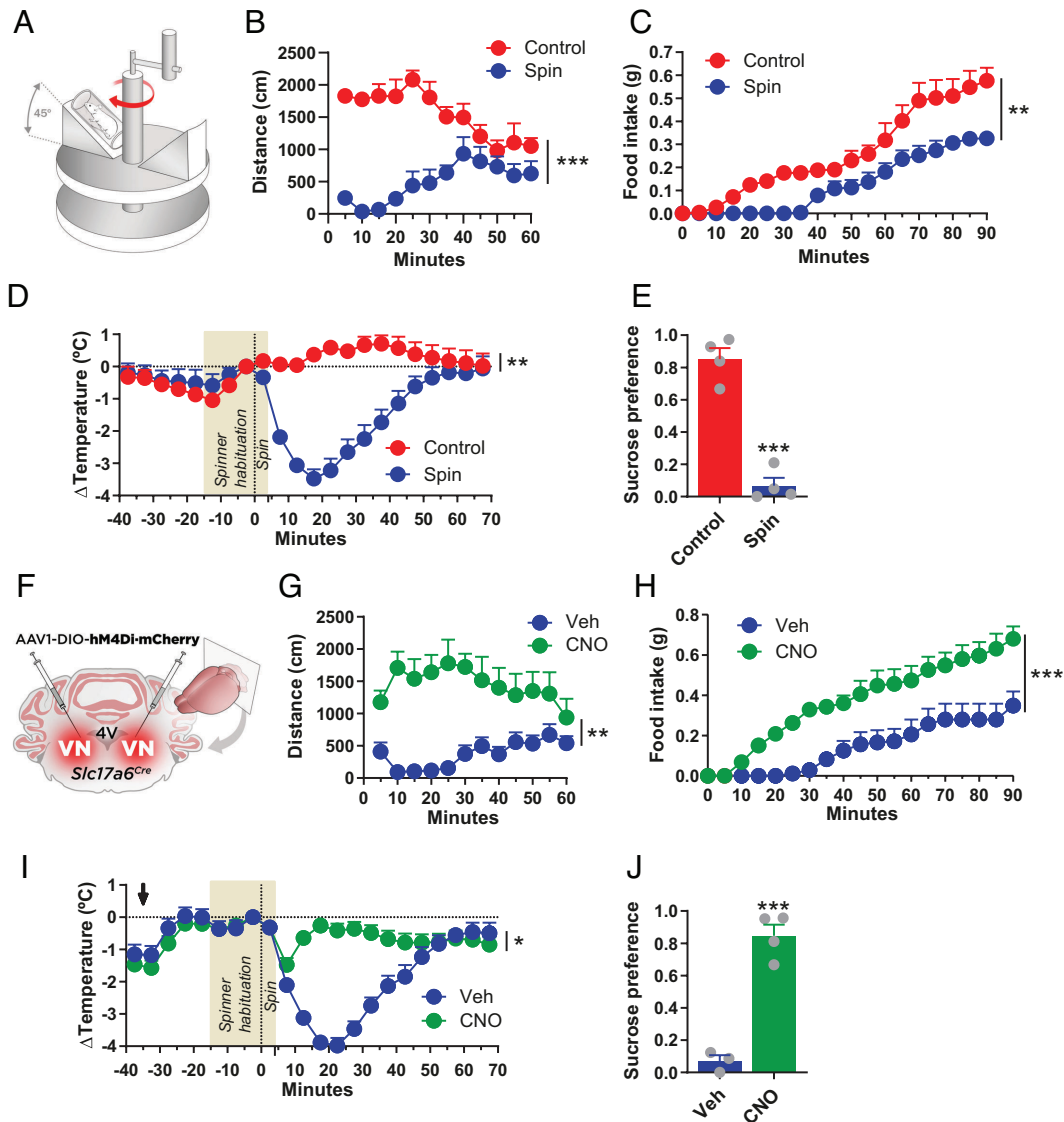


Fig. 1. VGLUT2^{VN} neuron inactivation blocks rotation-induced motion sickness-like symptoms in mice. (A) Mice were subjected to a rotational stimulus using a custom-made rotary device. The perpendicular distance from the mouse head to the axis of rotation was 5 cm. The mouse body inclination angle was 45°. (B) Traveled distance during a 60-min open-field test after spin or control stimulation (n = 6; two-way ANOVA, $P < 0.001$ effect of spin). (C) Cumulative food intake after spin or control stimulation (n = 6; two-way ANOVA, $P < 0.01$ effect of spin). Mice were food-deprived for 24 h prior to the test. (D) Body temperature difference (ΔT) after spin or control stimulation (n = 5; two-way ANOVA, $P < 0.01$ effect of spin). (E) CTA response in mice exposed to a two-bottle-based test pairing a 5% sucrose solution to rotational stimulus (n = 4; t test, $P < 0.001$). (F) *Slc17a6*^{Cre} mice were bilaterally injected in the VN with AAV1-DIO-hM4Di-mCherry (VGLUT2^{VN}:hM4Di mice) to inhibit glutamatergic neurons upon CNO administration. (G) Total distance traveled during a 60-min open-field session after spin stimulation in CNO- or vehicle-injected VGLUT2^{VN}:hM4Di mice (n = 10; two-way ANOVA, $P < 0.01$ effect of drug). (H) Cumulative food intake after spin stimulation in CNO- or vehicle-injected VGLUT2^{VN}:hM4Di mice (n = 7; two-way ANOVA, $P < 0.001$ effect of drug). Mice were food-deprived for 24 h prior to the test. (I) Core body temperature difference (ΔT) after spin stimulation in CNO- or vehicle-injected VGLUT2^{VN}:hM4Di mice (n = 4; two-way ANOVA, $P < 0.05$ effect of drug). The arrow shows the time of injection. (J) CTA response in mice exposed to a two-bottle-based test pairing a 5% sucrose solution to rotational stimulus in VGLUT2^{VN}:hM4Di mice injected with CNO (n = 4) or vehicle (n = 3) (t test, $P < 0.001$).

MS is known to induce a robust CTA (23). Hence, we asked whether rotation could establish a CTA in a two-bottle choice test (37). Two conditioning sessions pairing a 5% sucrose solution with rotational motion, were followed by a choice test of water or sucrose two days later. We observed a significant reduction in sucrose preference when sucrose was paired with rotation, compared to controls (Fig. 1E).

With the validity of the rotation paradigm established, we set out to define the neuronal substrate of vestibular-induced, MS-like responses. Excitatory neurons are highly abundant in the VN (30) and glutamatergic VN neurons are activated after provocative motion (35). Among the different glutamatergic markers, VGLUT2 (encoded by *Slc17a6*) shows a robust and significant expression in the VN (38), and VGLUT2-expressing neurons have been shown to participate in vestibular responses to hypergravity and postural imbalance, in contrast to GABAergic (VGAT-expressing) inhibitory neurons (31, 32). Thus, we assessed the necessity of genetically defined glutamatergic VGLUT2-expressing VN (VGLUT2^{VN}) neurons in eliciting MS behavioral and autonomic responses by bilateral chemogenetic inhibition in a well-characterized *Slc17a6*^{Cre} mouse line (39) (Fig. 1F and SI Appendix, Fig. S1C). Targeted chemogenetic inhibition of VGLUT2^{VN} neurons by expression of hM4Di and administration of clozapine N-oxide (CNO) had little effect on locomotion prior to spin stimulation (SI Appendix, Fig. S1D). However, inhibition of VGLUT2^{VN} neurons by CNO administration prevented spin-induced decreases in ambulatory activity (Fig. 1G), appetite suppression (Fig. 1H) and attenuated the MS-related decrease in body temperature (Fig. 1I). An initial decrease in body temperature was observed in CNO-injected mice, suggesting that other neuronal populations may contribute to the early spin-induced drop in body temperature. In addition, inhibition of VGLUT2^{VN} neurons also prevented spin-induced CTA (Fig. 1J). In contrast, bilateral chemogenetic inhibition of GABAergic (*Gad2*-expressing) VN neurons did not alter spin-induced hypolocomotion (SI Appendix, Fig. S1 E–G). These results indicate that VGLUT2^{VN} neurons are necessary to promote the development of the MS-like behavioral and autonomic responses elicited by rotational stimulation.

Nauseogenic responses can be obtained after unilateral inner ear caloric stimulation (40). Hence, to test whether VGLUT2^{VN} neuronal activation is sufficient to induce MS-like autonomic responses, *Slc17a6*^{Cre} mice received a unilateral injection of an AAV1 (adeno-associated viral) expressing Cre-dependent ChR2-YFP (VGLUT2^{VN}:ChR2 mice; for photoactivation) or a YFP construct (VGLUT2^{VN}:YFP mice; as control) into the right VN, and an optical fiber was implanted over the injected VN (Fig. 2A). Increased photostimulation frequencies ranging from 10 to 40 Hz, reduced ambulatory activity in VGLUT2^{VN}:ChR2 mice (SI Appendix, Fig. S1B). We used a 5-min, 40-Hz, optogenetic-stimulation paradigm because we and others have shown VGLUT2^{VN} neurons in actively moving mice maintain firing rates of up to 40 Hz (41, 42). VGLUT2^{VN} neuron optogenetic activation led to a significant decrease in spontaneous ambulatory activity (Fig. 2B), consistent with the results obtained after rotational stimulus. Pairing 5% sucrose solution to unilateral optogenetic activation of VGLUT2^{VN} neurons did not result in significant differences between the ChR2 and the YFP group (Fig. 2C), even though ingestion of their regular, low-calorie chow and water intake were significantly decreased after optogenetic VGLUT2^{VN} activation, showing complete suppression for as long as 30 min after laser onset (Fig. 2D and E). Noteworthy, a normal feeding pattern was observed after presentation of a highly palatable, chocolate-flavored, liquid diet to a separate cohort of laser-stimulated VGLUT2^{VN}:ChR2 mice (Fig. 2F), ruling out physical inability to feed but rather a

lack of motivational drive to consume regular chow or water. Core body temperature significantly decreased, with a maximum 3 °C drop occurring 17.5 min after laser onset (Fig. 2G). To assess whether the observed optogenetic-induced loss of core body temperature was due to a reduction in ambulatory activity in VGLUT2^{VN}:ChR2 mice, an additional optogenetic stimulation was applied under physical restraint. Under these conditions, core body temperature increased in VGLUT2^{VN}:YFP mice, likely due to restraint-induced stress responses. However, VGLUT2^{VN}:ChR2 mice still showed a significant drop in body temperature coincident with photostimulation (Fig. 2H). Thus, these results highlight that VGLUT2^{VN} neuron activation is sufficient to recapitulate most MS-induced symptoms.

Identification of *Crh*- and *Cck*-Expressing VGLUT2^{VN} Neuronal Subpopulations. To define VGLUT2^{VN}-neuron subpopulations, we performed viral vector-mediated RiboTag molecular profiling (43–45) in VN homogenates of *Slc17a6*^{Cre} mice injected with a RiboTag-expressing construct [AAV1-DIO-Rpl22:HA (44); Fig. 3A]. Transcripts enriched in VGLUT2^{VN} neurons were identified by differential expression analysis in RNA samples extracted from the RiboTag immunoprecipitates (IP; containing polysome-associated mRNAs from VGLUT2^{VN} neurons) and the input (I) of the immunoprecipitation (containing RNA from all the different cell types in the VN). Data analysis confirmed specific enrichment for *Slc17a6* (*Vglut2*) and depletion of inhibitory neuron mRNAs (*Gad2*) and non-neuronal transcripts (*Cnp* and *Gfap*) in the RiboTag IPs. In addition, there was a significant enrichment for candidate VGLUT2^{VN} neuron subpopulation markers such as *Cck*, *Crh*, *Adcyap1*, *Gal*, *Cbln1*, and *Coch* (Fig. 3B).

Among these, *Crh*- and *Cck*-expressing neurons have been shown to be involved in autonomic and nauseogenic responses (46, 47), highlighting the potential relevance of these neuronal populations in VN-mediated MS responses. Subsequent in situ hybridization assays confirmed the existence of scattered *Crh*-positive cells that colocalized with *Slc17a6* (SI Appendix, Fig. S2A) and an abundant population of *Cck*-expressing neurons, constituting >60% of all *Slc17a6*-expressing neurons (Fig. 3C and D). Noteworthy, a second population of *Cck*-expressing cells (~45% of the total) that colocalized with *Gad2* was observed (SI Appendix, Fig. S2B).

Activation of Vestibular *Cck*-Expressing Neurons Causes MS-Like Autonomic Responses. To test the necessity of vestibular *Crh*- or *Cck*-expressing neuronal populations (CRH^{VN} or CCK^{VN} neurons, respectively) in the development of MS-like signs, we injected *Crh*^{Cre} or *Cck*^{Cre} mice bilaterally in the VN with an AAV vector carrying Cre-dependent hM4Di-mCherry (SI Appendix, Figs. S3A and Fig. 4A). Chemogenetic inhibition of CRH^{VN} neurons did not induce any effect pre- or postspin on ambulatory activity (SI Appendix, Fig. S3B and C), indicating that they are not necessary to develop rotation-induced autonomic responses. Unexpectedly, bilateral chemogenetic inhibition of CCK^{VN} neurons significantly decreased ambulatory activity in the absence of rotational stimulus (Fig. 4B), which led to an inability to move after the spin (Fig. 4C). Reducing the volume of the inhibitory chemogenetic vector (from 0.35 μL to 0.2 μL) in the VN of *Cck*^{Cre} mice also led to a marked decrease in locomotion in the CNO-injected hM4Di group, ruling out a role for *Cck*-expressing neurons from neighboring nuclei (SI Appendix, Fig. S3D–F). Since CCK^{VN} neuron inhibition per se is sufficient to induce locomotor effects, further experiments using this approach were hindered. Thus, we sought to establish

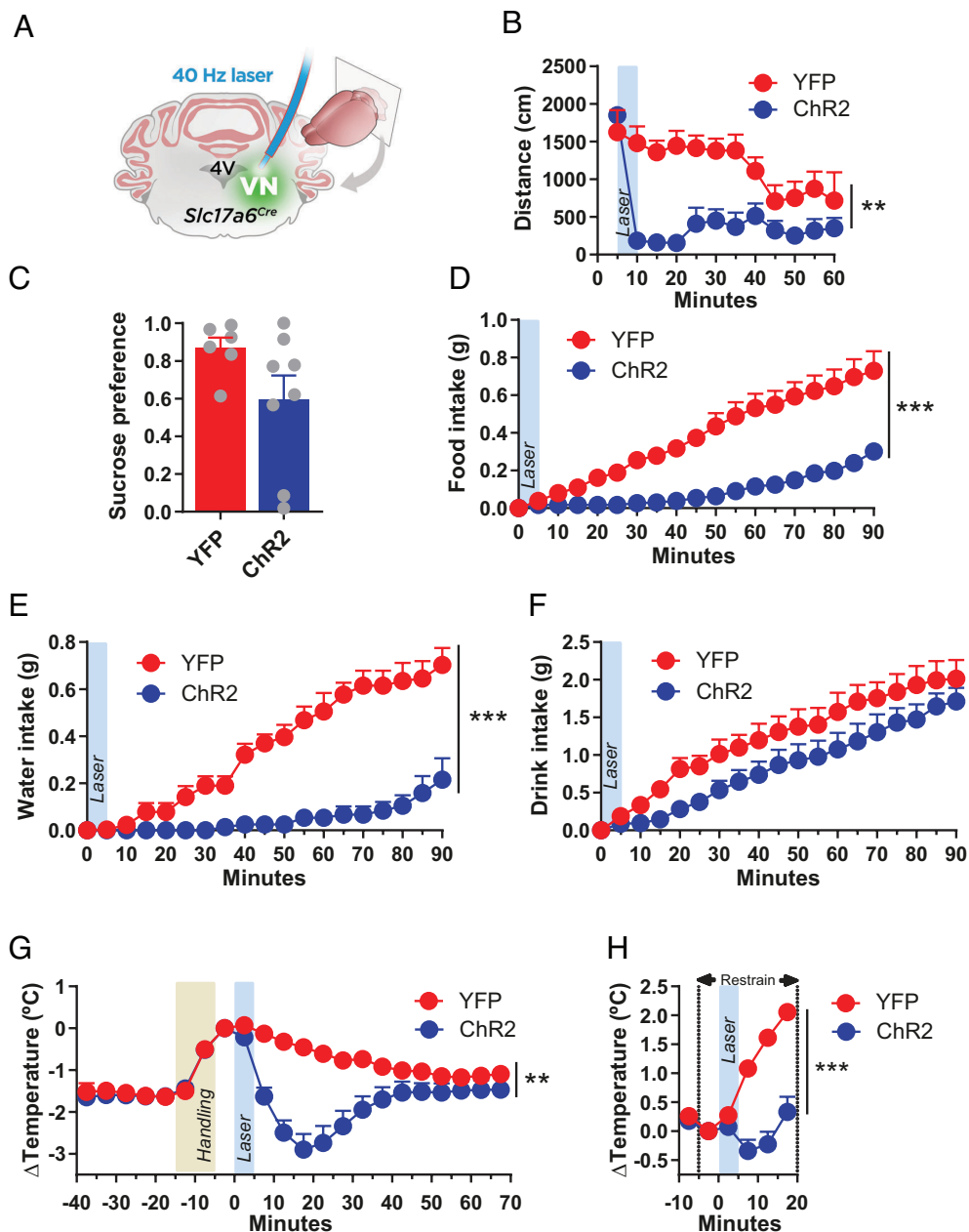


Fig. 2. VGLUT2^{VN} neuron activation is sufficient to induce motion sickness-like symptoms. (A) *Slc17a6^{Cre}* mice were unilaterally injected in the right VN with AAV1-DIO-ChR2-YFP (VGLUT2^{VN}:ChR2 mice) or AAV1-DIO-YFP (VGLUT2^{VN}:YFP mice), followed by optical fiber implantation over the right VN to deliver 40-Hz, 10-ms, 10-mW, 473-nm light pulses for 5 min under different behavioral approaches. (B) Distance traveled during 60 min of open-field test after photostimulation (VGLUT2^{VN}:ChR2 mice *n* = 7; VGLUT2^{VN}:YFP mice *n* = 5; two-way ANOVA, *P* < 0.01 effect of ChR2). (C) CTA response in mice exposed to a two-bottle-based test pairing a 5% sucrose solution to optogenetic activation of VGLUT2^{VN} neurons in VGLUT2^{VN}:ChR2 (*n* = 8) or control VGLUT2^{VN}:YFP (*n* = 6) mice (*t* test, *P* > 0.05). (D) Normal-chow intake following laser onset in VGLUT2^{VN}:ChR2 or VGLUT2^{VN}:YFP mice (*n* = 6; two-way ANOVA, *P* < 0.001 effect of ChR2). Animals were food-deprived for 24 h prior to photostimulation. (E) Water intake following laser onset in food-deprived, VGLUT2^{VN}:ChR2 or VGLUT2^{VN}:YFP mice (*n* = 6; two-way ANOVA, *P* < 0.001 effect of ChR2). (F) Highly palatable, chocolate-flavored drink intake following laser onset in food-deprived VGLUT2^{VN}:ChR2 or VGLUT2^{VN}:YFP animals (*n* = 6; two-way ANOVA, *P* > 0.05 effect of ChR2). (G) Core body temperature difference (ΔT) in freely moving VGLUT2^{VN}:ChR2 or VGLUT2^{VN}:YFP mice after handling and laser stimulation (*n* = 8; two-way ANOVA, *P* < 0.01 effect of ChR2). (H) Core body temperature difference (ΔT) in restrained VGLUT2^{VN}:ChR2 or VGLUT2^{VN}:YFP mice (*n* = 5; two-way ANOVA, *P* < 0.001 effect of ChR2). YFP: VGLUT2^{VN}:YFP mice; ChR2: VGLUT2^{VN}:ChR2 mice.

whether stimulation of CCK^{VN} neurons would be sufficient to elicit MS-like responses. Optogenetic activation of CCK^{VN} neurons (Fig. 4D), led to a significant and prolonged decrease in spontaneous ambulatory activity in the open-field (OF) test compared to the control animals (Fig. 4E) and the appearance of a robust CTA (Fig. 4F). Similarly, food intake was significantly decreased after photostimulation of CCK^{VN} neurons, showing a complete suppression for 35 min, while control animals engaged in feeding almost immediately (Fig. 4G). Optogenetic stimulation of CCK^{VN} neurons reduced core temperature (~4.5

°C), occurring 22.5 min after laser onset, in contrast to control mice (Fig. 4H). Thus, our results underscore that stimulation of CCK^{VN} neurons is sufficient to elicit MS-like behavioral and autonomic responses.

Since global CCK^{VN} inactivation alters normal VN function, likely by the combined action of neurotransmitters and neuropeptides, we also assessed the specific role of CCK (cholecystokinin) signaling blockade in spin-induced responses (Fig. 4I–K). Systemic administration of devazepide (Dev), a CCK-A receptor antagonist, prior to the rotation stimulus, was sufficient to block

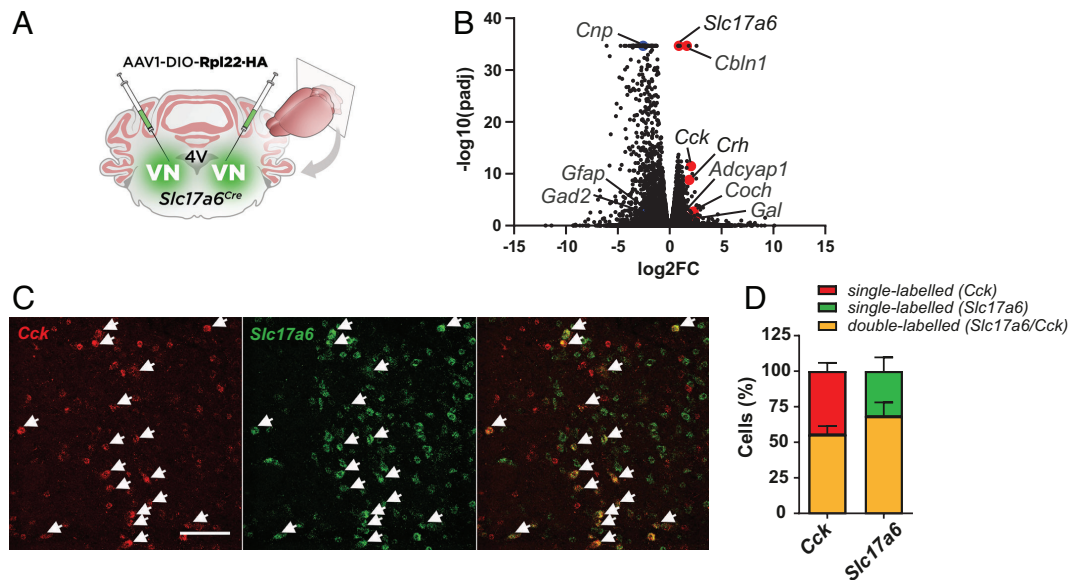


Fig. 3. Identification of glutamatergic neuronal subpopulations in the VN. (A) *Slc17a6^{Cre}* mice were bilaterally injected in the VN with a viral vector expressing the RiboTag (AAV1-DIO-Rpl22-HA) for the molecular profiling of VGLUT2^{VN} neurons. (B) Differential expression analysis showing significant enrichment for candidate VGLUT2^{VN} neuron subpopulation marker transcripts in the IPs of RiboTag assays when compared to inputs (n = 3). Specific enrichment for *Slc17a6* (*Vglut2*), and depletion for inhibitory neuron (*Gad2*) and non-neuronal marker transcripts (*Cnp*, *Gfap*) were confirmed in the analysis (padj: adjusted P-value; FC: fold change). (C) Double-label in situ hybridization assay showing expression of *Cck* mRNA within *Slc17a6*-expressing cells. (Scale bar: 100 μ m.) (D) Percentage of double-labeled *Cck*- and *Slc17a6*-expressing cells.

hypolocomotion (Fig. 4J) and the appearance of CTA (Fig. 4K), without having any overt behavioral prespin effects (Fig. 4J) other than an increase in food intake, as described (48, 49) (SI Appendix, Fig. S3G). In comparison, administration of dimenhydrinate (DMH), a common anti-MS antihistamine, was able to ameliorate spin-induced hypolocomotion only at 40 mg/kg, a dose that reduced locomotion prior to the rotatory stimulus (SI Appendix, Fig. S3H and I). These results reveal that vestibular CCK signaling can mediate MS-like behavioral and autonomic responses.

A CCK^{VN→PBN} Circuit Mediates MS-Like CTA Via CGRP (Calcitonin Gene-Related Peptide) Neuron Activation. We hypothesized that specific vestibular projections were likely driving discrete MS-induced responses. To elucidate the genetically defined, vestibular outputs involved in these responses, we compared the vestibular projections described in the Allen Mouse Brain Connectivity Atlas (121146455, 300687607) to the projection fields of *Slc17a6^{Cre}*, *Cck^{Cre}*, and *Gad2^{Cre}* mice injected with a Cre-dependent hM4Di-mCherry construct (SI Appendix, Table S1). Among the different brain regions, the PBN was consistently targeted in all animal groups (Fig. 5A), in agreement with the Allen Mouse Brain Connectivity Atlas and prior reports (27–29, 35, 50, 51). Furthermore, among brain areas showing robust CCK^{VN} axonal projections, both the VN and the PBN, but not the GRN, had more Fos-positive neurons after the rotational stimulus as assessed by immunohistochemistry (Fig. 5B and SI Appendix, Fig. S4A). Thus, these data confirmed the PBN as a prominent terminal field for VN neurons.

Our results pointed at an excitatory role for vestibuloparabrachial inputs. Accordingly, to identify the neuronal population in the PBN receiving inputs from VN neurons, we performed double-label ISH assays for *Fos* and *Calca* (which encodes the calcitonin gene-related peptide, CGRP) because these PBN neurons have been implicated in mediating visceral malaise and CTA (37, 52, 53). Results showed that spin stimulation induced *Fos* expression in *Calca*-expressing neurons (Fig. 5C). Thus, we hypothesized that a *Cck*-expressing vestibuloparabrachial (CCK^{VN→PBN}) circuit might be relevant in MS

by impinging onto CGRP^{PBN} neurons. To that end, we optogenetically activated CCK^{VN} axon terminals in the ipsilateral PBN by placing the optical fiber tip over this region in CCK^{VN}:ChR2 mice (Fig. 5D and SI Appendix, Fig. S5A). Photoactivation of CCK^{VN} neuronal terminals in the PBN increased the number of *Fos*-positive cells in the PBN, which colocalized with *Calca*-expressing neurons (Fig. 5E).

Behaviorally, optogenetic stimulation of CCK^{VN→PBN} fibers at 40 Hz significantly decreased sucrose preference when compared to controls (Fig. 5F), as well as body temperature (SI Appendix, Fig. S5B) without affecting locomotion or food intake (SI Appendix, Fig. S5C and D). Overall, these results underscore CCK^{VN→PBN} activation of CGRP neurons as a key component of MS-induced CTA. Quantification of activated CGRP^{PBN} neurons after rotational stimulus, as assessed by double ISH assays for *Fos* and *Calca* transcripts (Fig. 5G and H) showed that approximately 25% of CGRP^{PBN} neurons respond to spin. Antagonism of CCK-A receptor by Dev administration led to a 50% decrease in the percentage of active CGRP^{PBN} neurons after rotational stimulus (Fig. 5H) but did not significantly alter the number of *Fos*-expressing neurons in the VN (SI Appendix, Fig. S4B and C). Thus, our results identify a role for CCK-A signaling in the PBN for the development of MS responses.

Discussion

Being described by Hippocrates over 2000 y ago, MS affects millions of individuals (3). The CNS is thought to compute an MS-triggering sensory conflict signal analogously to “toxic shock”, eliciting malaise and nausea (6, 12, 25, 54). Thus, in an evolutionary context, MS responses could represent a proxy for toxicity-induced balance mismatches. Hence, vomiting observed in humans would be a response to evacuate toxic substances, appetite suppression to avoid additional toxic ingestion, hypolocomotion, and hypothermia to minimize the metabolism, and CTA to avoid consumption of toxins in the future. However, the neurobiological underpinnings of MS have remained elusive.

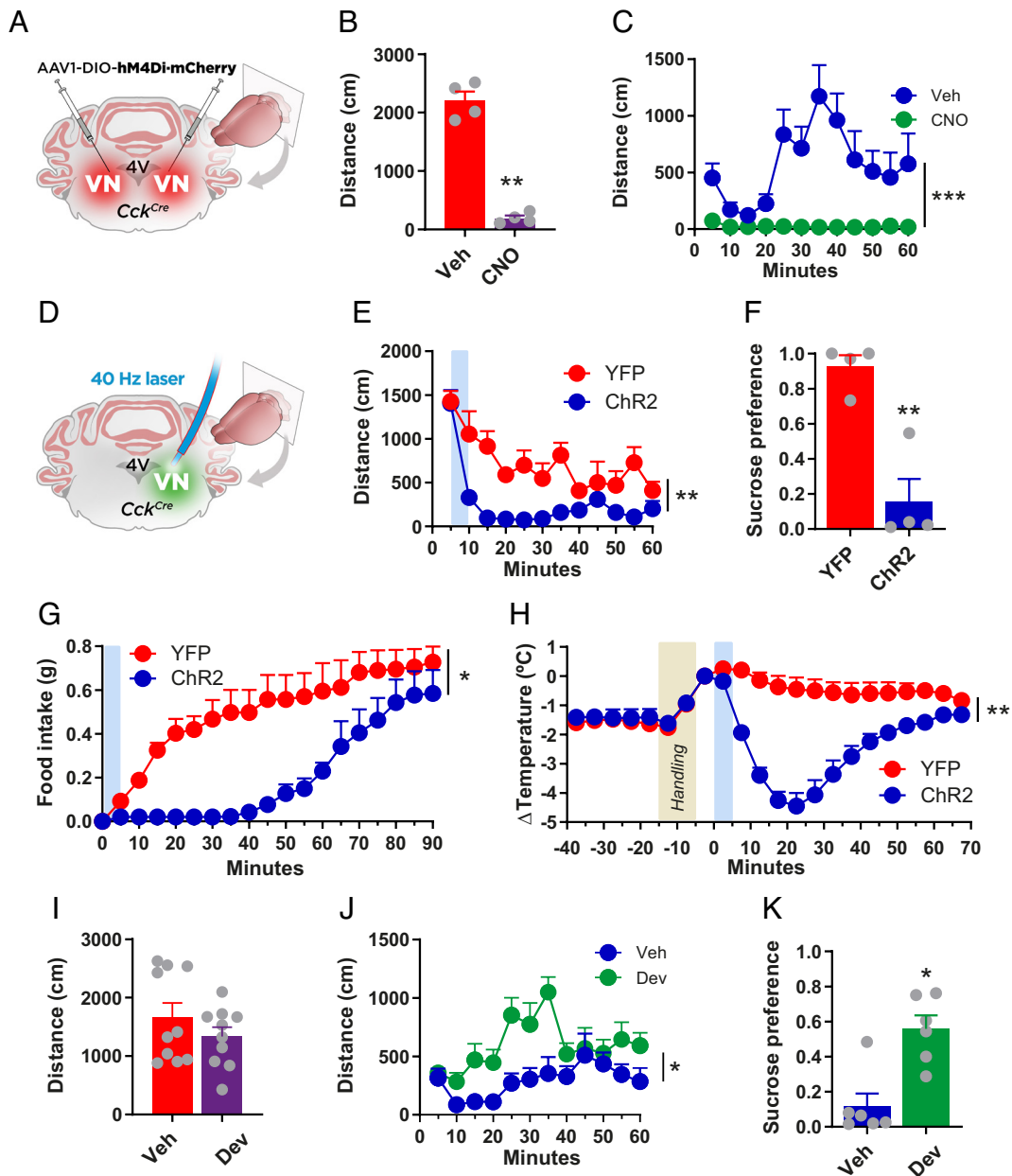


Fig. 4. CCK^{VN} neuron manipulation affects MS responses. (A) Cck^{Cre} mice were bilaterally injected in the VN with AAV1-DIO-hM4Di-mCherry (CCK^{VN}:hM4Di mice) to inhibit CCK^{VN} neurons upon CNO administration. (B) Five-minute OF test in CCK^{VN}:hM4Di mice 30 min after CNO or vehicle administration (n = 4; t test, P < 0.01). (C) OF test in CCK^{VN}:hM4Di mice injected with CNO or vehicle after spin stimulation (n = 4; two-way ANOVA, P < 0.001 effect of drug). (D) CCK^{Cre} mice were unilaterally injected in the right VN with AAV1-DIO-ChR2-YFP (CCK^{VN}:ChR2 mice) or AAV1-DIO-YFP (CCK^{VN}:YFP mice) followed by an optical fiber implantation to deliver a 5-min, 473-nm laser stimulation (40-Hz, 10-mW, 10-ms pulses). (E) OF test showing traveled distance after photostimulation in CCK^{VN}:ChR2 and CCK^{VN}:YFP mice (n = 4; two-way ANOVA, P < 0.01 effect of Chr2). (F) CTA response in mice exposed to a two-bottle-based test pairing a 5% sucrose solution to optogenetic activation of CCK^{VN} neurons in CCK^{VN}:ChR2 or control (CCK^{VN}:YFP) mice (n = 4; t test, P < 0.01). (G) Normal-chow intake after light stimulation in CCK^{VN}:ChR2 and CCK^{VN}:YFP mice. Mice were food-deprived for 24 h prior to stimulation (n = 4; two-way ANOVA, P < 0.05 effect of Chr2). (H) Core body temperature difference (ΔT) in CCK^{VN}:ChR2 and CCK^{VN}:YFP mice after handling and laser stimulation (n = 4; two-way ANOVA, P < 0.01 effect of Chr2). (I) Spontaneous ambulatory activity of mice 45 min after devazepide or vehicle administration in a 5-min, OF test (n = 10; t test, P > 0.05). (J) Traveled distance during 60 min of OF test after spin stimulation in devazepide or vehicle-treated mice (n = 10; two-way ANOVA, P < 0.05 effect of drug). (K) CTA response in devazepide or vehicle-treated mice exposed to a two-bottle-based test pairing a 5% sucrose solution to rotational stimulus (n = 6; t test, P-value < 0.05).

Our results link VGLUT2^{VN} and CCK^{VN} neuronal populations to the development of MS-like symptoms in mice. Furthermore, we reveal a CCK^{VN}→PBN projection that is sufficient to induce CTA and hypothermia likely through the activation of an ensemble of PBN neurons that express the CCK-A receptor including *Calca*-expressing neurons. Our results suggest the potential use of CCK-A receptor blockers as a treatment for MS.

MS is conserved among animal phyla (4, 6–9), but with a high degree of heterogeneity in its behavioral and physiological

correlates. Mice do not present an emetic reflex but do present overt physiological and behavioral alterations when exposed to a nauseogenic experience (4, 17, 18, 23, 24, 55) such as sustained 2-g rotational stimuli (8, 16–18, 24, 31). We show that an intermittent rotational stimulus of 4 min is sufficient to develop robust hypolocomotion, hypophagia, hypothermia, and CTA.

The role of the VN in the development of MS is well recognized (16, 17). The currently accepted hypothesis is that the vestibular inner ear organs provide a major input for the subsequent

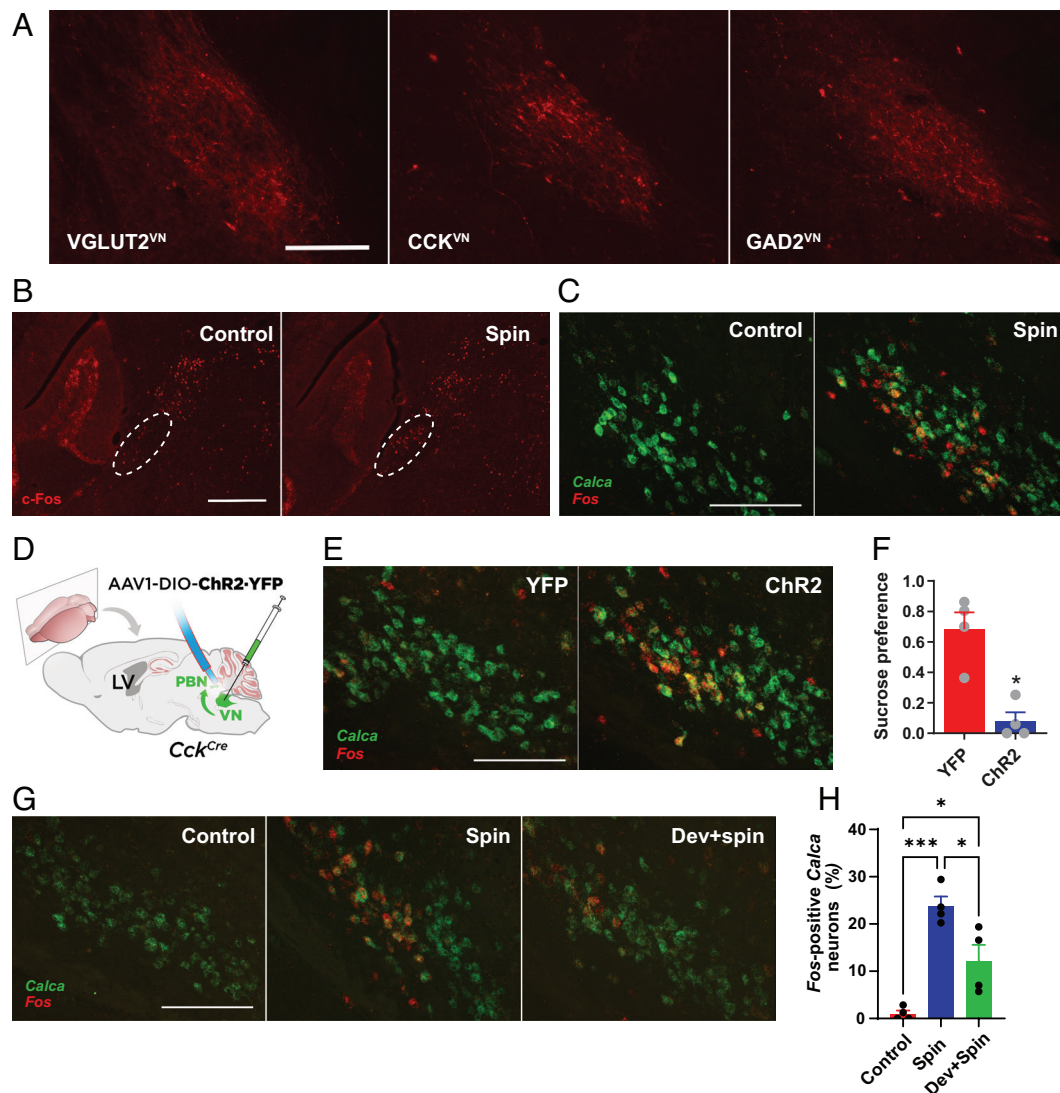


Fig. 5. CCK^{VN} neurons target the PBN to mediate CTA. (A) Representative images at Bregma -5.2 mm showing projections to the PBN from VGLUT2^{VN}, CCK^{VN}, and GAD2^{VN} neurons as assessed by hM4Di:mCherry visualization in sections containing the PBN from VGLUT2^{VN}:hM4Di, CCK^{VN}:hM4Di, and GAD2^{VN}:hM4Di mice. (Scale bar: 150 μ m.) (B) Fos staining at Bregma -5.2 mm from mice subjected to spin or control stimulation. The dotted line delineates lateral PBN. (Scale bar: 400 μ m.) (C) Double-label in situ hybridization assay (RNAscope) showing expression of Fos mRNA within Calca-expressing neurons in the PBN after rotational stimulation. (Scale bar: 250 μ m.) (D) Illustration showing AAV1-DIO-ChR2-YFP or AAV1-DIO-YFP injection in the VN and optical fiber implantation over the PBN in Cck^{Cre} mice for photoactivation of CCK^{VN} neuron projections in the PBN (CCK^{VN}→PBN). (E) Double-label in situ hybridization assay (RNAscope) showing expression of Fos mRNA within Calca-expressing neurons in the PBN after photoactivation of CCK^{VN}→PBN projections (scale bar: 250 μ m). (F) CTA response in mice exposed to a two-bottle-based test pairing a 5% sucrose solution to targeted optogenetic activation of the CCK^{VN}→PBN circuit in CCK^{VN}:ChR2 (n = 3) or control (CCK^{VN}:YFP; n = 4) mice (t test, $P < 0.05$). (G) Double-label in situ hybridization assay (RNAscope) showing expression of Fos mRNA within Calca-expressing neurons in the PBN of control or spin-stimulated mice with or without Dev (1 mg/kg) administration (scale bar: 250 μ m). (H) Quantification of the percentage of Fos-positive Calca-expressing cells in the PBN of control or spin-stimulated mice with or without Dev (1 mg/kg) administration (n = 4; one-way ANOVA, * $P < 0.05$, *** $P < 0.001$).

computing comparisons between present sensory input (integrated input including vestibular, visual, and proprioceptive information) and memory recalled from similar motion situations experienced in the past (12, 13). Rotational stimuli convey information from the semicircular canals mostly onto medial VN (MVN) neurons, leading to nauseogenic responses (5, 40, 56). Previous studies had identified that VGLUT2^{VN} neurons, highly abundant in the VN (30), participate in postural balance and mediate gravitational stress-induced hypolocomotion, hypophagia, and hypothermia (31, 32). Here, we confirm that these results show that VGLUT2^{VN} neurons are necessary for the development of MS responses, such as CTA, in a rotational paradigm in mice. Our results show that while unilateral optogenetic activation of VGLUT2^{VN} neurons elicits the responses, bilateral chemogenetic inhibition of the same populations does not have the converse effect on locomotion,

which may suggest that a glutamatergic drive is necessary to elicit vestibular-induced effects on locomotion. Alternatively, bilateral inhibition may result in the absence of conflicting commissural inhibition, thus limiting the effects on locomotion (49).

Several excitatory populations have been described in the VN that may be involved in different aspects of vestibular-mediated responses (57). Using the RiboTag approach (43, 45) we identified several genetic markers for subpopulations. Our results validate genes *Crh* and *Adcyap1* (57) and identify additional markers for VGLUT2^{VN} neurons including *Gal*, *Coch*, and *Cck*. Furthermore, we provide evidence that *Cck*-expressing neurons are the most abundant glutamatergic vestibular neuronal population.

At the functional level, we show that unilateral optogenetic activation of CCK^{VN} neurons is sufficient to recapitulate MS-induced responses, such as hypolocomotion, hypothermia, and

hypophagia, and to elicit a robust CTA. On the other hand, restricted chemogenetic inhibition of CCK^{VN} neurons significantly decreased ambulatory activity and temperature, even in the absence of a rotational stimulus. Different mechanisms may account for this paradoxical response. First, VN presents a high degree of compensation, such as contralateral commissural inhibition (58). Thus, alterations in neuronal activity may lead to compensatory contralateral activation. However, compensatory responses were neither observed after VGLUT2^{VN}, GAD2^{VN} nor CRH^{VN} inhibition, pointing at a specific role of CCK^{VN} neurons. In this regard, we have uncovered the existence of both glutamatergic and GABAergic CCK^{VN} neurons. This fact, given the existence of GABAergic local and commissural interneurons as well as GABAergic projection populations (59) may underlie the strong effect observed after CCK^{VN} activity modulation. Alternatively, MVN neurons produce endogenous, spontaneous pacemaker activity (60). Restoration of MVN pacemaker activity is key for MS habituation (61). Thus, it may be possible that CCK^{VN} neurons contribute to pacemaker activity and alterations in their rhythmic firing rate may lead to MS-like symptoms. Alternatively, it is possible that either activation or inhibition of these neurons affects balance, which may secondarily cause the MS responses. Future studies assessing the contribution of balance per se are warranted.

At the circuitry level, our results underscore genetically defined, target- and density-specific projections that may underlie their differential contribution to MS-induced responses. Of the different axonal projections, we describe dense projections from CCK^{VN} neurons to the PBN. The PBN is known to mediate malaise, appetite suppression, lethargy, anxiety, thermoregulation, and CTA (26, 55, 62). Chemogenetic inhibition of VGLUT2^{VN} neurons blocked hypothermia and CTA in our MS paradigm. Unilateral optogenetic stimulation of CCK^{VN} neurons or their projections to the PBN produced hypothermia and robust CTA, which is not recapitulated by optogenetic activation of VGLUT2^{VN} neurons, which may suggest the existence of parallel, or opposing, VGLUT2^{VN} neuronal populations/pathways. In contrast, activation of VGLUT2^{VN} neurons leads to hypothermia, likely by decreasing sympathetic tone (31). Recent reports revealed that *Pdyn*-expressing PBN neurons (PDYN^{PBN}) regulate hypothermia through projections to the preoptic area (62), involved in temperature regulation (63). Hence, CCK^{VN} activation of PDYN^{PBN} neurons might mediate the MS-induced drop in body temperature.

Rotational stimulus and CCK^{VN} optogenetic stimulation activated CGRP-expressing, glutamatergic neurons in the lateral PBN, which are known to be involved in malaise, and CTA (26), sustaining the establishment of aversive taste memories (37). Thus, we propose that glutamatergic CCK^{VN} input onto CGRP^{PBN} neurons mediates MS-induced CTA. CCK^{VN}→PBN projections do not seem to participate in MS-induced hypophagia and hypoactivity, even though activation of CGRP^{PBN} neurons is involved in appetite suppression and reduced locomotion (26, 64, 65). Thus, it is likely that CCK^{VN} projections to other brain areas may be responsible for these responses. For example, CCK^{VN} neurons also project to the NTS, which contains neurons that can activate PBN^{CGRP} neurons to promote anorexia (66). Alternatively, it is possible that unilateral CCK^{VN}→PBN activation was not sufficient to recruit a large population of CGRP^{PBN} neurons. Accordingly, our results show that ~25% of PBN^{CGRP} neurons respond to CCK^{VN}→PBN projection activation. Given that different PBN^{CGRP} subpopulations have been recently described (67), this may indicate that only specific subsets of PBN^{CGRP} are targeted by CCK^{VN}→PBN projections. Alternatively, while CTA is commonly referred to as conditioned taste aversion, we acknowledge that we have not assessed other unequivocal signs of aversion (such as gapes

and chin rubs) or malaise. Thus, the responses observed may be due to conditioned avoidance, rather than aversion, which are two independent processes (68), which may also explain the absence of a hypophagic response after CCK^{VN}→PBN stimulation.

Our data show that alterations in the activity of CCK^{VN} neurons exert a pivotal role in controlling MS-like behavioral responses. Here, we provide several lines of evidence that CCK signaling, through its CCK-A receptor, underlies MS responses. Dev administration abolishes both hypolocomotion and CTA after a rotational stimulus, without affecting spontaneous locomotion like DMH, a widely used anti-MS drug.

Pharmacologically, three anti-MS drug classes have been described depending on their influence over MS habituation. Thus, class A drugs such as amphetamine are thought to block the MS-eliciting sensory input, leading to habituation delay. Class B drugs such as anticholinergics modulate the neural store decreasing the neuronal mismatch signal intensity, leading to boosted habituation. On the other hand, class C drugs such as antihistamines inhibit MS-related autonomic responses, leading to unchanged MS habituation (69). Even though we have not tested habituation per se, our results suggest that Dev may be preventing the expression of autonomic responses, akin to class C drugs. Mechanistically, we show that CCK-A receptor blockade reduces CGRP^{PBN} activation, in agreement with our recent study reporting the expression of *Cckera* in CGRP^{PBN} neurons (67). In addition to its known gastric effects, CCK-A receptor signaling has been suggested to contribute to multiple central functions, such as anxiety, nociception, and food consumption (70).

Our study underscores a key role for CCK^{VN} neurons in MS-related behavioral and physiologic responses by impinging onto PBN circuitry, providing evidence of a direct link between motion inputs and aversive responses. Furthermore, we identify CCK-A receptor blockade as a therapeutic approach for MS. Future studies detailing the behavioral and physiological contribution of other CCK^{VN} targets will provide a more complete profile of the neurobiological substrates of MS.

Methods

Mice. The following mouse lines were used in this study: *Slc17a6^{Cre}* (BAC-Vglut2-Cre) (39) mice were generated by Ole Kiehn. *Cck^{Cre}* (CCK-IRES-Cre), and *Crh^{Cre}* (CRH-IRES-Cre) (71) mice were obtained from The Jackson Laboratory (Bar Harbor, ME. Stock No: 012706 and 012704, respectively). Mice were group-housed with a 12:12h light:dark cycle at 22 °C, with ad libitum access to rodent chow (Teklad Global Rodent Diet #2014S; Envigo) and water, unless otherwise stated. Sex and age-balanced groups of 2- to 7-month-old mice were used across all experimental procedures. No sex differences were observed. After surgeries, animals were individually housed until the end of all experimental procedures. Sample sizes were determined using power analyses. The number of animals used per group in each experiment (n) is provided in figure legends. All mice were on a C57BL/6J background after backcrossing for at least 10 generations. All experiments were conducted following the recommendations in the Guide for the Care and Use of Laboratory Animals and were approved by the Animal Care and Use Committee of the Universitat Autònoma de Barcelona and the Generalitat de Catalunya.

Drugs. Dev (Tocris #2304, 1 mg/kg in saline solution containing 1% Dimethyl Sulphoxide and 1% Tween-80) and DMH (Merck #PHR1658, 20 or 40 mg/kg in saline solution) were administered intraperitoneally (i.p.) 45 or 30 min before tests, respectively. A between-subject design was used for pharmacologic studies, with animals receiving either Veh-Drug or Drug-Veh in a balanced manner (SI Appendix, Fig. S6).

Rotational Stimulus. Prior to rotational stimulation, animals were habituated to physical restraint for 4 min using a 50-mL conical tube coupled to a custom-made rotary device (external radius: 10.5 cm; internal radius from mouse head: 5 cm. Rotation multiplier: ×3.6). Afterward, rotational (four repeated 1-min, 4-g

accelerations) or control (4 min with no rotation) stimuli were applied, unless otherwise stated. One-minute accelerations included 55 s of rotation plus 5 s break until full stop. To achieve 4-*g* accelerations, 75 rpm was applied.

Behavioral Assays. Each animal was subjected to an OF test, followed by food intake and conditioned taste aversion (CTA) analysis. After tests, telemetric temperature sensors were implanted, and core-body temperature was monitored.

Open Field (OF) Test. The OF test was conducted in a noncovered, white methacrylate box (56 × 36.5 × 31 cm) that allows for video recording during animal testing. Mice were individually exposed for 5 min to the OF before receiving rotational or control stimulation. After stimulation, mice were reexposed to the OF for 60 more min. For optogenetic experiments, mice were exposed for a total of 60 min to the OF (5 min of prestimulation, followed by 5 min of laser stimulation and 50 min of poststimulation). Spontaneous ambulatory activity was monitored using video tracking software (Ethovision XT 11.5; Noldus Information Technology).

Food and Liquid Intake Measurement. Animals were individually placed in an OxyletPro-PhysioCage monitoring system (Panlab) for real-time quantification of food and liquid intake. Mice were habituated to the cage for 2 to 4 d with ad libitum access to normal chow and water, unless otherwise stated. Prior to each session, animals were food-deprived for 24 h and refed at the onset of the dark cycle. For specific experiments, chocolate-flavored, highly palatable liquid diet (ENSURE Nutrivigor, Abbott) was provided during cage habituation and in the subsequent experimental sessions. Food and liquid intake were expressed as cumulative intake using the Metabolism software version v3.0.00 (Panlab).

Conditioned-Taste Avoidance (CTA) test. For the CTA test, a two bottle-based protocol was used (37). Animals were individually placed in a custom cage with angular ports for two liquid-containing bottles. Ad libitum water access was provided for 2 d during habituation. Next, animals only had access to both water-containing bottles during restricted time periods (30 min access in the morning and 30 to 60 min in the afternoon) for 8 d (D1 to D8). During days 4 and 6 (D4 and D6), a solution of 5% sucrose in water was paired with specific stimuli (rotation, CNO injection, photostimulation) to establish conditioning. Mice were tested on D8. The sucrose preference value was calculated as sucrose solution consumption/total liquid consumption.

Surgical Implantation of Telemetry Devices and Temperature Monitoring. Anesthetized mice (5% isoflurane for induction and 1.5% for maintenance) were aseptically implanted with telemetric temperature transmitters (G2 E-Mitter, STARR Life Sciences Corp.) into the peritoneum and allowed to recover for 2 wk. Mouse cages were placed on telemetry receivers (ER4000 Energizer/Receiver, STARR Life Sciences Corp.), and core body temperature was monitored using the VitalView software version 5.0 (STARR Life Sciences Corp.) under controlled ambient temperature (22 °C). All recordings started in resting animals. For specific experiments, mice were inserted into a modified 50-mL Falcon tube to ensure physical restraint while allowing optogenetic tethering.

Viral Vector Production. pAAV-hSyn-DIO-hM4Di-mCherry, pAAV-EF1a-DIO-eYFP, and pAAV-EF1a-DIO-ChR2-YFP plasmids were obtained from Addgene (#44362, #27056, and #100056, respectively). pAAV RiboTag virus (pAAV-EF1a-DIO-Rpl22-HA) has been described (44). Recombinant AAV vectors were produced in human embryonic kidney (HEK293T) cells with AAV1 coat serotype. Purification was achieved by several sucrose and CsCl gradient centrifugations and a final resuspension in 1 × Hanks Balanced Saline Solution at a titer of 2×10^9 viral genomes/ μ L as described (44, 72). AAV preparations were aliquoted and stored at -80 °C until stereotaxic injection.

Stereotaxic Surgery. All surgeries were performed under aseptic conditions. Animal anesthesia was induced and maintained with 5% and 1 to 1.5% isoflurane/ O_2 , respectively. Analgesia (5 mg/kg ketoprofen; Sanofi-Aventis) and ocular protective gel (Viscotears[®], Bausch+Lomb) were applied. Mice were then placed over a heating pad in a robot-operated, 3-dimensional (stereotaxic) frame (Neurostar) for intracerebral virus delivery. Stereotaxic coordinates were normalized using a correction factor (Bregma-Lambda distance/4.21) based on the coordinates of Paxinos and Franklin (73). AAV preparations were unilaterally (right side) or bilaterally delivered into the VN [antero-posterior (AP), -6.00 mm from Bregma;

medio-lateral (ML), ± 0.90 mm; dorso-ventral (DV), -4.00 mm from skull surface) at a constant rate of 0.1 μ L/min for 3.5 to 4.0 min (0.20 to 0.40 μ L per injection site) using a 32-gauge blunt needle coupled to a 5- μ L syringe (Hamilton). After infusion, the needle was maintained in place for 6 min to allow proper diffusion. Subsequent needle withdrawal was performed at 1 mm/min to ensure minimal off-target viral leakage. After viral injection, mice used for optogenetic experiments also received unilateral surgical implantation of a fiber-optic cannula as described below. Only animals with correct targeting were included in the experiment (SI Appendix, Fig. S7).

Chemogenetics. *Slc17a6^{Cre}*, *Cck^{Cre}*, or *Crh^{Cre}* mice were bilaterally injected in the VN with 0.35 μ L (per side) of AAV1-hSyn-DIO-hM4Di-mCherry. Clozapine-*n*-oxide (CNO; 1 mg/kg) was administered via i.p. injection 35 min prior to rotational or control stimulation. A between-subject design was used for chemogenetics studies, with animals receiving either Veh-CNO or CNO-Veh in a balanced manner (SI Appendix, Fig. S6).

Optogenetics. *Slc17a6^{Cre}* or *Cck^{Cre}* mice were injected in the right VN with 0.4 μ L of either AAV1-EF1 α -DIO-ChR2-YFP or AAV1-EF1 α -DIO-eYFP and a fiber-optic cannula (200- μ m fiber core diameter, 0.22-numeric aperture; 2.5-mm ferrule diameter; Thorlabs) was implanted over the right VN (AP, -6.00 mm; ML, $+0.90$ mm; DV, -4.00 mm) or over the right PBN (AP, -5.20 mm; ML, $+1.70$ mm; DV, -3.00 mm) of *Cck^{Cre}* animals. A fiber-optic cannula was fixed to the exposed skull with a layer of adhesive cement (Super-Bond C&B, Sun Medical) and dental acrylic cement (Rebaron, GC Corporation). The skin was affixed to the cement with tissue adhesive (Vetbond, 3M). A blue 473-nm laser light was produced by a DPSS Laser System (LRS-0473-GFM-00100-05 Laserglow) and driven by a fiber-optic patch cord (200- μ m core diameter, 0.22-numeric aperture: FT030 protection, Thorlabs). Light intensity was set at 10 mW measured by a photometer (Thorlabs) at the tip of a nonimplanted fiber optic cannula attached to the patch-cord. To deliver illumination to the right VN or right PBN, the patch cord was connected to the implanted fiber-optic-containing cannula through a ceramic sleeve. A pulse generator (33500B Series Trueform, Keysight) was used to adjust laser output to deliver 40-Hz, 10-ms, pulse trains for 5 min to all mice.

Mapping of Neuronal Projections. To visualize the projections of VGLUT2^{VN}, CCK^{VN}, or GAD2^{VN} neurons, *Slc17a6^{Cre}*, *Cck^{Cre}*, or *Gad2^{Cre}* mice were injected into the right VN with 0.2 μ L of AAV1-hSyn-DIO-hM4Di-mCherry. Animals were killed 3 wk after surgery for direct visualization of fibers after tissue fixation and cryopreservation.

Tissue Processing and Immunofluorescence Analysis. Mouse brains were freshly dissected following CO₂ asphyxia, fixed overnight with phosphate-buffered saline (PBS) containing 4% paraformaldehyde, and cryoprotected with 30% sucrose in PBS. For cryosectioning, brains were frozen for 5 min in dry ice and sectioned in a freezing microtome. For immunofluorescence, 30- μ m free-floating sections were blocked in PBS with 10% normal donkey serum (NDS) and 0.2% Triton X-100 for 1 h at room temperature followed by an overnight incubation at 4 °C with primary antibody solution containing a rabbit anti-c-Fos (1:1,000; #ab222699, Abcam) antibody in PBS with 1% NDS and 0.2% Triton X-100. After three washes in PBS with 0.2% Triton X-100, a secondary antibody solution containing a secondary antibody conjugated to Alexa Fluor 594 fluorophore (1:500; Invitrogen) was added to the sections and incubated for 1 h at room temperature. After the incubation, sections were washed three times for 5 min in PBS with 0.2% Triton X-100 and mounted onto slides with DAPI Fluoromount (#17984-24, Electron Microscopy Sciences) before visualization with an EVOS imaging system (Thermo Fisher Sci).

RiboTag Assays. For genetic identification of neuronal subsets, *Slc17a6^{Cre}* mice were bilaterally injected in the VN with 0.4 μ L of the RiboTag viral vector (AAV1-DIO-Rpl22-HA) (44). Animals were euthanized 3 wk after surgery for subsequent RiboTag analysis. To isolate the polysome-associated mRNAs from VGLUT2^{VN} neurons, punches containing the VN of *Slc17a6^{Cre}* mice injected with AAV1-DIO-Rpl22-HA were pooled and homogenized in 1 mL of buffer as described (45). After centrifugation, 4 μ L of anti-HA antibody (MMS-101R, 2 to 3 mg/mL; Covance) was added to 800 μ L of the cleared lysate and incubated for 4 h at 4 °C. The remaining lysate was saved as input sample. After incubation, 200 μ L of protein A/G magnetic beads (Thermo Scientific) was added and incubated overnight at 4 °C

with rotation. IPs were washed in high-salt buffer and RNA from inputs and IPs were extracted (43). For differential expression analysis, 10 ng of RNA was amplified using the Ovation Pico SL WTA system (NuGEN). The fidelity of amplification was confirmed by qPCR analysis of the resulting cDNA using the QuantiTect kit (Qiagen) before biotinylation according to the EncoreL biotinylation kit (NuGEN). Biotinylated cDNA was quantified, and product size distribution was analyzed using the 2100 Bioanalyzer system with the RNA 6000 Nano chips (Agilent Technologies). Biotinylated cDNA (750 ng) was hybridized at 48 °C to MouseRef-8 v2 expression beadchips (Illumina) for 16 h before washing and analyzing according to the manufacturer's directions. Signal was detected using a BeadArray Reader (Illumina), and data were analyzed for differential expression using the GenomeStudio data analysis software (Illumina). Average normalization, the Illumina custom error model, and multiple testing corrections using the Benjamini-Hochberg false discovery rate were applied to the analysis. Only transcripts with a differential score of >13 ($P < 0.05$) were considered.

In Situ Hybridization Assays. Mouse brains were fresh-frozen in Tissue-Tek O.C.T. compound (Sakura) with dry ice and stored at -80°C until cryosectioning. Coronal sections (15 μm) containing the VN or the PBN were used for RNAscope (Advanced Cell Diagnostics) analysis following the manufacturer's directions. The following probes were used: Mm-*Slc17a6* (#319171-C3), Mm-*Cck* (#402271-C2), Mm-*Crh* (#316091-C1), Mm-*Gad2* (#439371-C1), Mm-*Fos* (#316921-C1), and Mm-*Calca* (#578771-C2). All in situ hybridization assays were imaged using a confocal (Leica SP5) or epifluorescence (Nikon Eclipse 90i) microscope and analyzed in ImageJ (Fiji v1.0) or QuPath open-source software (74). Cell counting was performed in VN sections from Bregma -5.68mm to -6.64mm in 2 to 3 slices/animal ($n = 3$ animals) with the ImageJ Cell Counter plugin (Fiji v1.52). The number of Fos-positive *Calca*-expressing cells was analyzed using QuPath. Cell segmentation was accomplished in DAPI-stained sections containing *Calca*-expressing neurons from Bregma -5.02mm to -5.34mm using the cell detection feature with a cell expansion of 30 μm . After cell detection, Fos and *Calca* transcripts were detected using the subcellular detection module. Each section was visually inspected to confirm accurate spot identification. The number of Fos-positive *Calca*-expressing cells was obtained from 2 to 5 sections per mouse with 4 mice per group.

Statistics. Data are shown as the mean \pm SEM. GraphPad Prism v9.0 software was used for statistical analyses. Appropriate tests were selected depending on the experimental design as stated in the figure legends. Statistical significance, when reached ($P < 0.05$ was considered significant), is stated in the figure legends. The number of mice in an experiment (n) represents the number of animals per group. Different cohorts of mice were assigned to different tests to avoid undergoing repeated testing. No attrition was observed.

Data, Materials, and Software Availability. All study data are included in the article and/or *SI Appendix*. Microarray normalized and raw data can be accessed through GEO Series Accession number [GSE167672](https://www.ncbi.nlm.nih.gov/geo/query/acc.cgi?acc=GSE167672) (75).

ACKNOWLEDGMENTS. We thank Diane Durnam for editing the manuscript. This work was supported by a Network of European Neuroscience Schools exchange grant for training stay (P.M.-M), a Marie Skłodowska-Curie Individual Fellowship (H2020-MSCA-IF-2014-658352; E.S.), predoctoral fellowships (2018FI_B00452 to A.U.; PRE2018-083179 to L.S.-B, PRE2021-096944 to M.G.), and three Ramón y Cajal fellowships (RyC-2012-11873; A.Q., RYC2019-028501-I; E.S., RYC2020-029596-I; E.P.). E.P. received funds from MICINN (PID2021-125079OA-I00). E.S. received funds from MICIU Projectos I+D+i "Retos Investigación" (RTI2018-101838-J-I00) and MICINN Projectos I+D+i (PID2019-107633RB-I00 and PID2022-1425440B-I00). A.Q. received funds from the European Research Council (Starting grant NEUROMITO, ERC-2014-StG-638106), MINECO Projectos I+D de Excelencia (SAF2014-57981P; SAF2017-88108-R), MICINN Projectos I+D+i (PID2020-114977RB-I00), AGAUR (2017SGR-323, 2021SGR-720), Fundació TV3-La Marató (202030), and "la Caixa" Foundation (ID 100010434), under the agreement LCF/PR/HR20/52400018.

Author affiliations: ^aInstitut de Neurociències, Universitat Autònoma de Barcelona, Barcelona 08193, Spain; ^bDepartment of Cell Biology, Physiology and Immunology, Universitat Autònoma de Barcelona, Barcelona 08193, Spain; ^cHIMI, University of Washington, Seattle, WA 98195; ^dDepartment of Biochemistry, University of Washington, Seattle, WA 98195; and ^eFocus Area for Human Metabolomics, Faculty of Natural and Agricultural Sciences, North-West University, Potchefstroom 2520, South Africa

- Bertolini, D. Straumann, Moving in a moving world: A review on vestibular motion sickness. *Front. Neurol.* **7**, 14–14 (2016).
- Graybiel, C. D. Wood, E. F. Miller, D. B. Cramer, Diagnostic criteria for grading the severity of acute motion sickness. *Aerospace Med.* **39**, 453–455 (1968).
- K. E. Money, Motion sickness. *Physiol. Rev.* **50**, 1–39 (1970).
- E. Nalivaiko, "Thermoregulation and nausea" in *Handbook of Clinical Neurology*, A. A. Romanovsky, Ed. (Elsevier, 2018), vol. **156**, pp. 445–456.
- F. H. Previc, Do the organs of the labyrinth differentially influence the sympathetic and parasympathetic systems? *Neurosci. Biobehav. Rev.* **17**, 397–404 (1993).
- M. Treisman, Motion sickness: An evolutionary hypothesis. *Science* **197**, 493–495 (1977).
- K. Helling, S. Hausmann, A. Clarke, H. Scherer, Experimentally induced motion sickness in fish: Possible role of the otolith organs. *Acta Otolaryngol.* **123**, 488–492 (2003).
- S. Ngampramuan *et al.*, Thermoregulatory correlates of nausea in rats and musk shrews. *Oncotarget* **5**, 1565–1575 (2014).
- X. Wei *et al.*, Verification of motion sickness index in mice. *CNS Neurosci. Therapeut.* **17**, 790–792 (2011).
- J. R. Lackner, Motion sickness: More than nausea and vomiting. *Exp. Brain Res.* **232**, 2493–2510 (2014).
- W. Bles, J. E. Bos, B. de Graaf, E. Groen, A. H. Wertheim, Motion sickness: Only one provocative conflict? *Brain Res. Bull.* **47**, 481–487 (1998).
- J. T. Reason, Motion sickness adaptation: A neural mismatch model. *J. R. Soc. Med.* **71**, 819–829 (1978).
- C. M. Oman, "Sensory conflict in motion sickness: An observer theory approach" (NASA, Ames Research Center, Spatial Displays and Spatial Instruments, 1991), Pictorial communication in virtual and real environments, pp. 362–376.
- W. James, The sense of dizziness in deaf-mutes. *Am. Ann. Deaf Dumb* **28**, 102–117 (1883).
- J. A. Irwin, The pathology of sea-sickness. *The Lancet* **118**, 907–909 (1881).
- C. Abe, K. Tanaka, C. Iwata, H. Morita, Vestibular-mediated increase in central serotonin plays an important role in hypergravity-induced hypophagia in rats. *J. Appl. Physiol.* **109**, 1635–1643 (2010).
- D. M. Murakami, L. Erkmann, O. Hermanson, M. G. Rosenfeld, C. A. Fuller, Evidence for vestibular regulation of autonomic functions in a mouse genetic model. *Proc. Natl. Acad. Sci. U.S.A.* **99**, 17078–17082 (2002).
- Z. H. Zhang *et al.*, A new vestibular stimulation mode for motion sickness with emphatic analysis of pica. *Front. Behav. Neurosci.* **16**, 882695 (2022).
- M. Dieterich *et al.*, Medial vestibular nucleus lesions in wallenberg's syndrome cause decreased activity of the contralateral vestibular cortex. *Ann. N. Y. Acad. Sci.* **1039**, 368–383 (2005).
- D. E. Angelaki, K. E. Cullen, Vestibular system: The many facets of a multimodal sense. *Annu. Rev. Neurosci.* **31**, 125–150 (2008).
- B. J. Yates, M. J. Holmes, B. J. Jian, Adaptive plasticity in vestibular influences on cardiovascular control. *Brain Res. Bull.* **53**, 3–9 (2000).
- B. J. Yates, A. D. Miller, Properties of sympathetic reflexes elicited by natural vestibular stimulation: Implications for cardiovascular control. *J. Neurophysiol.* **71**, 2087–2092 (1994).
- J. J. Braun, H. McIntosh, Learned taste aversions induced by rotational stimulation. *Physiol. Psychol.* **1**, 301–304 (1973).
- P. M. Fuller, T. A. Jones, S. M. Jones, C. A. Fuller, Neurovestibular modulation of circadian and homeostatic regulation: Vestibulohypothalamic connection? *Proc. Natl. Acad. Sci. U.S.A.* **99**, 15723–15728 (2002).
- E. Nalivaiko, J. A. Rudd, R. H. Y. So, Motion sickness, nausea and thermoregulation: The "toxic" hypothesis. *Temperature* **1**, 164–164 (2014).
- R. D. Palmiter, The parabrachial nucleus: CGRP neurons function as a general alarm. *Trends Neurosci.* **41**, 280–293 (2018).
- C. D. Balaban, Vestibular nucleus projections to the parabrachial nucleus in rabbits: Implications for vestibular influences on the autonomic nervous system. *Exp. Brain Res.* **108**, 367–381 (1996).
- C. D. Balaban, G. Beryozkin, Vestibular nucleus projections to nucleus tractus solitarius and the dorsal motor nucleus of the vagus nerve: Potential substrates for vestibulo-autonomic interactions. *Expe. Brain Res.* **98**, 200–212 (1994).
- S. Liu *et al.*, Divergent brainstem opioidergic pathways that coordinate breathing with pain and emotions. *Neuron* **110**, 857–873.e9 (2022).
- E. Erő, M.-O. Gewaltig, D. Keller, H. Markram, A cell atlas for the mouse brain. *Front. Neuroinform.* **12**, 84–84 (2018).
- C. Abe *et al.*, VGLUT2-expressing neurons in the vestibular nuclear complex mediate gravitational stress-induced hypothermia in mice. *Commun. Biol.* **3**, 227 (2020).
- Q. Montardy *et al.*, Selective optogenetic stimulation of glutamatergic, but not GABAergic, vestibular nuclei neurons induces immediate and reversible postural imbalance in mice. *Prog. Neurobiol.* **204**, 102085 (2021).
- G. R. Holstein, V. L. Friedrich Jr., G. P. Martinelli, Glutamate and GABA in vestibulo-sympathetic pathway neurons. *Front. Neuroanat.* **10**, 7 (2016).
- A. H. Gagliuso, E. K. Chapman, G. P. Martinelli, G. R. Holstein, Vestibular neurons with direct projections to the solitary nucleus in the rat. *J. Neurophysiol.* **122**, 512–524 (2019).
- Y.-L. Cai *et al.*, Glutamatergic vestibular neurons express Fos after vestibular stimulation and project to the NTS and the PBN in rats. *Neurosci. Lett.* **417**, 132–137 (2007).
- P. Singh, S. S. Yoon, B. Kuo, Nausea: A review of pathophysiology and therapeutics. *Ther. Adv. Gastroenterol.* **9**, 98–112 (2016).
- J. Y. Chen, C. A. Campos, B. C. Jarvie, R. D. Palmiter, Parabrachial CGRP neurons establish and sustain aversive taste memories. *Neuron* **100**, 891–899.e5 (2018).
- L. Ng *et al.*, An anatomic gene expression atlas of the adult mouse brain. *Nat. Neurosci.* **12**, 356–362 (2009).

39. L. Borgius, C. E. Restrepo, R. N. Leao, N. Saleh, O. Kiehn, A transgenic mouse line for molecular genetic analysis of excitatory glutamatergic neurons. *Mol. Cell. Neurosci.* **45**, 245–257 (2010).
40. H. F. Lidvall, Mechanisms of motion sickness as reflected in the vertigo and nystagmus responses to repeated caloric stimuli. *Acta Otolaryngol.* **55**, 527–536 (1962).
41. I. Bolea *et al.*, Defined neuronal populations drive fatal phenotype in a mouse model of Leigh syndrome. *Elife* **8**, e47163 (2019).
42. W. Waespe, V. Henn, The velocity response of vestibular nucleus neurons during vestibular, visual, and combined angular acceleration. *Exp. Brain Res.* **37**, 337–347 (1979).
43. E. Sanz, J. C. Bean, D. P. Carey, A. Quintana, G. S. McKnight, RiboTag: Ribosomal tagging strategy to analyze cell-type-specific mRNA expression in vivo. *Curr. Protoc. Neurosci.* **88**, e77 (2019).
44. E. Sanz *et al.*, Fertility-regulating Kiss1 neurons arise from hypothalamic POMC-expressing progenitors. *J. Neurosci.* **35**, 5549–5556 (2015).
45. E. Sanz *et al.*, Cell-type-specific isolation of ribosome-associated mRNA from complex tissues. *Proc. Natl. Acad. Sci. U.S.A.* **106**, 13939–13944 (2009).
46. R. F. Parrott, I. S. Ebenezer, B. A. Baldwin, M. L. Forsling, Central and peripheral doses of cholecystokinin that inhibit feeding in pigs also stimulate vasopressin and cortisol release. *Exp. Physiol.* **76**, 525–531 (1991).
47. M. J. Nijssen *et al.*, The role of the CRH type 1 receptor in autonomic responses to corticotropin-releasing hormone in the rat. *Neuropsychopharmacology* **22**, 388–399 (2000).
48. I. S. Ebenezer, Effects of intracerebroventricular administration of the CCK(1) receptor antagonist devazepide on food intake in rats. *Eur. J. Pharmacol.* **441**, 79–82 (2002).
49. N. Bellissimo, G. H. Anderson, Cholecystokinin-A receptors are involved in food intake suppression in rats after intake of all fats and carbohydrates tested. *J. Nutr.* **133**, 2319–2325 (2003).
50. X. Shi *et al.*, Whole-brain monosynaptic inputs and outputs of glutamatergic neurons of the vestibular nuclei complex in mice. *Hear. Res.* **401**, 108159 (2021).
51. S. S. Horowitz, J. Blanchard, L. P. Morin, Medial vestibular connections with the hypocretin (orexin) system. *J. Comp. Neurol.* **487**, 127–146 (2005).
52. C. A. Campos *et al.*, Cancer-induced anorexia and malaise are mediated by CGRP neurons in the parabrachial nucleus. *Nat. Neurosci.* **20**, 934–942 (2017).
53. M. E. Carter, S. Han, R. D. Palmiter, Parabrachial calcitonin gene-related peptide neurons mediate conditioned taste aversion. *J. Neurosci.* **35**, 4582–4586 (2015).
54. I. L. Bernstein, Learned taste aversions in children receiving chemotherapy. *Science* **200**, 1302–1303 (1978).
55. Z. Xie *et al.*, The gut-to-brain axis for toxin-induced defensive responses. *Cell* **185**, 4298–4316.e21 (2022).
56. F. H. Previc, Intravestibular balance and motion sickness. *Aerosp. Med. Hum. Perform.* **89**, 130–140 (2018).
57. T. Kodama *et al.*, Neuronal classification and marker gene identification via single-cell expression profiling of brainstem vestibular neurons subserving cerebellar learning. *J. Neurosci.* **32**, 7819–7831 (2012).
58. N. Mano, T. Oshima, H. Shimazu, Inhibitory commissural fibers interconnecting the bilateral vestibular nuclei. *Brain Res* **8**, 378–382 (1968).
59. S. M. Highstein, G. R. Holstein, The anatomy of the vestibular nuclei. *Prog. Brain Res.* **151**, 157–203 (2006).
60. Y. Lin, D. O. Carpenter, Medial vestibular neurons are endogenous pacemakers whose discharge is modulated by neurotransmitters. *Cell. Mol. Neurobiol.* **13**, 601–613 (1993).
61. L. Ris, B. Capron, N. Vibert, P. P. Vidal, E. Godaux, Modification of the pacemaker activity of vestibular neurons in brainstem slices during vestibular compensation in the guinea pig. *Eur. J. Neurosci.* **13**, 2234–2240 (2001).
62. A. J. Norris, J. R. Shaker, A. L. Cone, I. B. Ndiokho, M. R. Bruchas, Parabrachial opioidergic projections to preoptic hypothalamus mediate behavioral and physiological thermal defenses. *Elife* **10**, e60779 (2021).
63. C. L. Tan *et al.*, Warm-sensitive neurons that control body temperature. *Cell* **167**, 47–59.e15 (2016).
64. M. E. Carter, M. E. Soden, L. S. Zweifel, R. D. Palmiter, Genetic identification of a neural circuit that suppresses appetite. *Nature* **503**, 111–114 (2013).
65. A. J. Bowen *et al.*, Dissociable control of unconditioned responses and associative fear learning by parabrachial CGRP neurons. *Elife* **9**, e59799 (2020).
66. C. W. Roman, V. A. Derkach, R. D. Palmiter, Genetically and functionally defined NTS to PBN brain circuits mediating anorexia. *Nat. Commun.* **7**, 11905 (2016).
67. J. L. Pauli *et al.*, Molecular and anatomical characterization of parabrachial neurons and their axonal projections. *Elife* **11**, e81868 (2022).
68. L. A. Parker, Taste avoidance and taste aversion: Evidence for two different processes. *Learn. Behav.* **31**, 165–172 (2003).
69. N. Takeda *et al.*, Neural mechanisms of motion sickness. *J. Med. Invest.* **48**, 44–59 (2001).
70. S. Ballaz, The unappreciated roles of the cholecystokinin receptor CCK(1) in brain functioning. *Rev. Neurosci.* **28**, 573–585 (2017).
71. H. Taniguchi *et al.*, A resource of Cre driver lines for genetic targeting of GABAergic neurons in cerebral cortex. *Neuron* **71**, 995–1013 (2011).
72. A. Quintana *et al.*, Fatal breathing dysfunction in a mouse model of Leigh syndrome. *J. Clin. Invest.* **122**, 2359–2368 (2012).
73. K. B. J. Franklin, G. Paxinos, *Paxinos and Franklin's The mouse brain in stereotaxic coordinates* (Academic Press, an imprint of Elsevier, Amsterdam, ed. 4, 2013), vol. 1.
74. P. Bankhead *et al.*, QuPath: Open source software for digital pathology image analysis. *Sci. Rep.* **7**, 16878 (2017).
75. E. Sanz, A. Quintana, Gene expression profiling of Vglut2 neurons in the vestibular nucleus (VN). Gene Expression Omnibus. <https://www.ncbi.nlm.nih.gov/geo/query/acc.cgi?acc=GSE167672>. Deposited 27 February 2021.